ChemPubSoc Europe

DOI: 10.1002/cctc.201901964

CHEMCATCHEM Full Papers

Three-Enzyme Phosphorylase Cascade Immobilized on Solid Support for Biocatalytic Synthesis of Cello–oligosaccharides

Chao Zhong,[a] Božidar Duić,[a] Juan M. Bolivar,[a] and Bernd Nidetzky*[a, b]

Enzyme cascades are promising for multistep biocatalytic synthesis, but their effective use beyond the proof-of-concept stage is challenging. Strategies to recycle the individual enzymes are critical for the applicability of such cascades. Immobilization on solid support is well developed for single enzymes but remains difficult for enzyme ensembles. Here, we show a controlled co-immobilization of three glycoside phosphorylases to establish a highly active and recyclable biocatalyst for the conversion of sucrose and glucose into soluble (short-chain) cello–oligosaccharides. We use protein fusion with the binding module Z_{basic2} to enable non-covalent surface tethering of all enzymes according to a uniform principle and in a programmable fashion. We thus achieve loading of the phosphorylases in an activity ratio optimal for the overall conversion and for controlling the cello–oligosaccharide chain length ($\leq$6), hence the solubility, in the reaction. We demonstrate efficient production of ~12 g/L cello–oligosaccharides with integrated enzyme re-use, retaining ~85% of the overall initial activity after five reaction cycles. This study presents a major advance toward the practical use of systems bio-catalysis on solid support.

Introduction

To provide energy and promote biosynthesis, cellular metabolism relies fundamentally on a highly interconnected system of enzymatic reactions organized in multistep cascades.[1] Adopting the natural principle in practical form, systems bio-catalysis seeks to develop multienzyme cascades for the application in organic synthesis.[2] The general concept is appealing for the promise held, that complex multistep chemical transformations can be performed in one pot without the need to isolate reaction intermediates.[3] Furthermore, advanced strategies of reaction engineering (e.g. recycling of catalytic reagents;[4] removal of inhibitors;[4–5] displacement of reaction equilibrium;[6] improved process control[3c,7]) can be integrated effectively via suited cascade design. Although met with high interest in many fields of bio-catalysis,[2a,6c,8] multienzyme cascades have played particularly important roles in synthetic carbohydrate chemistry focused on the assembly of defined oligosaccharide structures.[9] One-pot multienzyme-catalyzed transformations were central in order to gain access to such oligosaccharides, several of which, including low-molecular weight heparin[10] and human milk oligosaccharides,[11] have attracted considerable attention for commercial use. Enzyme cascades have recently been also adopted for the automated oligosaccharide synthesis.[12]

The significant promise of "telescoped" biocatalytic reactions notwithstanding, enzyme cascades have yet to see actual uses in oligosaccharide production. Lack of application, and the resulting underuse of their potential, stems from perceived limitations on the applicability of such cascades from the process chemistry point of view.[2b,5a,13] To operate the enzyme cascades efficiently at larger scale is a considerable challenge. Their complexity necessitates a large set of interdependent reaction parameters be properly balanced. One major hurdle in making enzyme cascades fit for production is to manage the recycling of the whole enzyme ensemble for multiple rounds of conversion. Traditionally, enzyme recycling is handled through immobilization on solid supports.[14] Such technology is well developed for single enzymes but is not similarly advanced for enzyme ensembles.[6a,14d,15]

Immobilization of multiple enzymes can be achieved by immobilizing the enzymes individually, each on its own suited support,[16] or by co-immobilization of all the enzymes used on a single support.[6a,14d,15,17] Co-immobilization approaches can be further distinguished according to whether the principle used for immobilization is enzyme-specific or uniform.[6a,16b,18] Thoughtful comparisons of the benefits and drawbacks of immobilization strategies for multiple enzymes have been presented in comprehensive reviews,[6a,14d,15,17a] and successful applications of each principal type of immobilization approach

[a] Dr. C. Zhong, B. Duić, Dr. J. M. Bolivar, Prof. Dr. B. Nidetzky
Institute of Biotechnology and Biochemical Engineering
Graz University of Technology, NAWI Graz
Petersgasse 12, 8010 Graz (Austria)
E-mail: bernd.nidetzky@tugraz.at
[b] Prof. Dr. B. Nidetzky
Austrian Centre of Industrial Biotechnology
Petersgasse 14, 8010 Graz (Austria)

Supporting information for this article is available on the WWW under https://doi.org/10.1002/cctc.201901964

This publication is part of a joint Special Collection with ChemBioChem on "Excellence in Biocatalysis Research". Please follow the link for more articles in the collection.

have been reported.[15b,17a,18b,19] Generally, immobilization of multiple enzymes on the same carrier may be useful to exploit the effects of spatial proximity.[6a,14d,17,20] "Individualized" strategies of enzyme immobilization facilitate enzyme-specific optimization of activity or stability.[14d,21] Due to its facile use, uniform co-immobilization is promising for the accelerated development of enzyme cascades on solid supports. Advanced strategies of modular enzyme engineering via fusion protein approaches (see below) extend the scope of multienzyme co-immobilization by a uniform principle of enzyme-surface tethering. In this study, therefore, a fusion protein-enabled approach to enzyme cascade co-immobilization was pursued.

In the field of carbohydrates, an important approach by Wang and co-workers demonstrated co-immobilization of enzyme cascades for sugar nucleotide synthesis.[22] The so-called "sugar beads" involved tethering of multiple enzymes via their His-tag. The His-tag, like other short peptide tags widely used in protein purification, is convenient for the combined purification and immobilization of enzymes.[23] However, the efficiency of the tags in protein tethering to surfaces can vary widely depending on the enzyme used and is challenging to predict.

Here, we present an effective and flexible strategy for the controlled co-immobilization of the individual enzymes from a biocatalytic cascade. We use chimeric proteins obtained by fusion of the binding module Z_{basic2} to the enzymes of interest.[24] The Z_{basic2} module is small (58 amino acids; ~7 kDa, Supporting Information) and folds autonomously into a three α-helical bundle structure. Due to multiple arginine residues exposed on one of its sides (Figure 1A), the Z_{basic2} has considerable affinity for the binding to the negatively charged solid surfaces, such as those of cation exchange resins and silica materials.[24d,25] We demonstrate that fusion with the Z_{basic2} empowers enzyme co-immobilization with excellent modularity and control that are both crucial factors of practical efficiency in immobilizing multiple enzymes; and are quite challenging to attain by merely combining individual enzyme-specific immobilization protocols.[26] Important elements of control in the Z_{basic2} mediated immobilization are enzyme orientation on the solid surface[24b] and relative amount of different enzymes loaded onto the carrier. Previous studies show that the enzymes immobilized via Z_{basic2} are uniformly distributed within porous particles.[24]

Based on the approach just outlined, we here develop a three-enzyme biocatalytic cascade of glycoside phosphorylases (sucrose phosphorylase, ScP, EC 2.4.1.7; cellobiose phosphorylase, CbP, EC 2.4.1.20; cellodextrin phosphorylase, CdP, EC 2.4.1.49) co-immobilized on solid support. We use this cascade to synthesize soluble cello–oligosaccharides (degree of polymerization, DP ≤ 6) via chain-length controlled, iterative β-1,4-glucosylation of glucose from sucrose (Figure 1B,C). The cello–oligosaccharides are known as functional dietary fibers for food[27] and feed[28] use and their assembly via bottom-up elongation of glucose is promising for large-scale production.

As shown in Figure 1C, the cascade reaction involves α-glucose 1-phosphate (αGlc 1-*P*), released from sucrose and phosphate by ScP, as donor substrate for the consecutive β-1,4-glucosylations by CbP and CdP.[29] Previous study of the three-enzyme cascade in solution shows, that shuttling of the glucosyl residues to and from phosphate constitutes an important factor of conversion efficiency.[30] To avoid cello–oligosaccharide precipitation during reaction in solution, tight control of DP in product is additionally required.[29,31] Without such control, the CdP would elongate the growing oligosaccharide chains until they become largely insoluble.[32] Besides reaction time, the activity ratio of the three phosphorylases is another critical process parameter. The consequent requirement to fine-tune the individual enzyme activities on the support poses a fundamentally difficult challenge for the enzyme co-immobilization to establish. Our study shows that the Z_{basic2}-directed immobilization can overcome the current limitations and thus enables an efficient production of soluble cello–oligosaccharide with integrated re-use of enzymes. Overall, the results have broad relevance for the practical use of systems bio-catalysis on solid support.

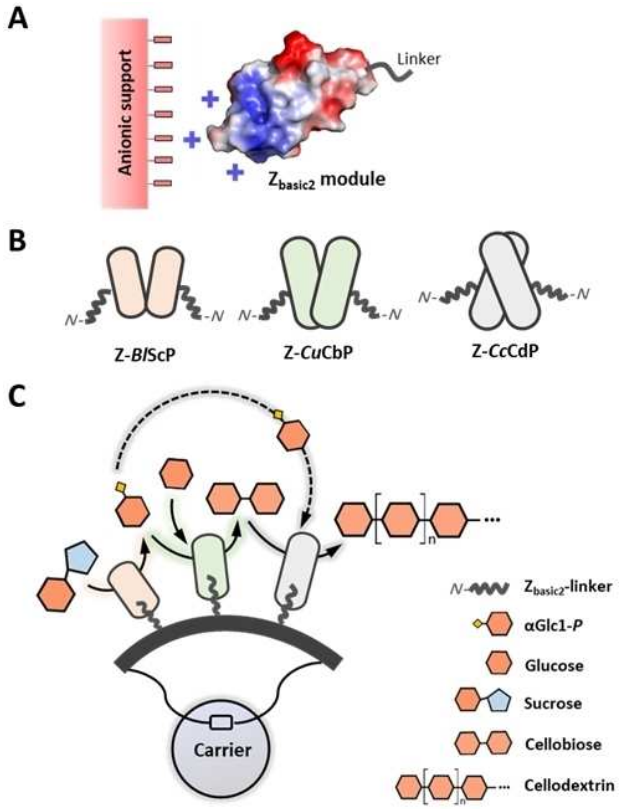

Figure 1. Phosphorylase co-immobilization using a platform of Z–enzyme fusions. A) The Z_{basic2} binding module. B) Chimeric glycoside phosphorylases harboring the Z_{basic2} module at their N-terminus. The position of Z_{basic2} module inferred from the dimeric enzyme structures is shown schematically. C) Three-enzyme phosphorylase cascade on solid support for the synthesis of cello–oligosaccharides from sucrose and glucose. A phosphate/α-glucose 1-phosphate shuttle is used for an iterative β-1,4-glucosylation to elongate glucose via cellobiose into a cello–oligosaccharide chain. Enzyme binding on the negatively charged surface of porous carriers occurs primarily via Z_{basic2} module, thus enabling convenient co-immobilization of two or three enzymes according to a uniform principle of surface tethering.

Results and Discussion

Modular Z–enzyme platform of glycoside phosphorylases

We constructed N-terminal fusions with the Z_{basic2} module of the cellobiose phosphorylase from *Cellulomonas uda* (Z–*Cu*CbP) and the cellodextrin phosphorylase from *Clostridium cellulosi* (Z–*Cc*CdP).[29] Analysis of structure models (Supporting Information, Figure S1) suggested the N-terminus as the proper location for the Z_{basic2} module in both enzymes, for it would be placed far away from the active site and should, in general, be accommodated well in protein structure (Figure 1B). We obtained the corresponding Z-fusion of ScP from *Bifidobacterium longum* (Z–*Bl*ScP) from an earlier study,[26b] in which we showed that the N-terminally placed Z_{basic2} module was not interfering with the enzyme activity. All the phosphorylases used here are functional homodimers in solution. The quaternary structure organization duplicates the Z_{basic2} modules available for Z–enzyme surface tethering (Figure 1B). Bivalency in protein-surface interaction resulting from two Z_{basic2} modules present in the enzyme molecule (e.g., Z–enzyme dimer, Z–Z–enzyme, Z–enzyme–Z) was previously shown to benefit the enzyme immobilization, through increased loading and more stable binding.[26b]

The Z–*Cu*CbP and Z–*Cc*CdP were obtained from *Escherichia coli* overexpression culture and purified by cation exchange chromatography, as previously reported for Z–*Bl*ScP[26b] and described in full detail in the Supporting Information. The two enzymes showed the expected molecular mass for their full-length protein subunit including Z_{basic2} (Figure S4). The specific activities of purified Z–*Cu*CbP and Z–*Cc*CdP were 15 U/mg and 17 U/mg, respectively, corresponding to the specific activities of the corresponding reference (i.e., N-terminally His-tagged) enzymes within a twofold range. The specific activity of Z–*Bl*ScP was 84 U/mg, in agreement with earlier work.[26b] We thus concluded that each Z–enzyme was suitable for the study of its individual immobilization as well as of its co-immobilization with the other enzymes.

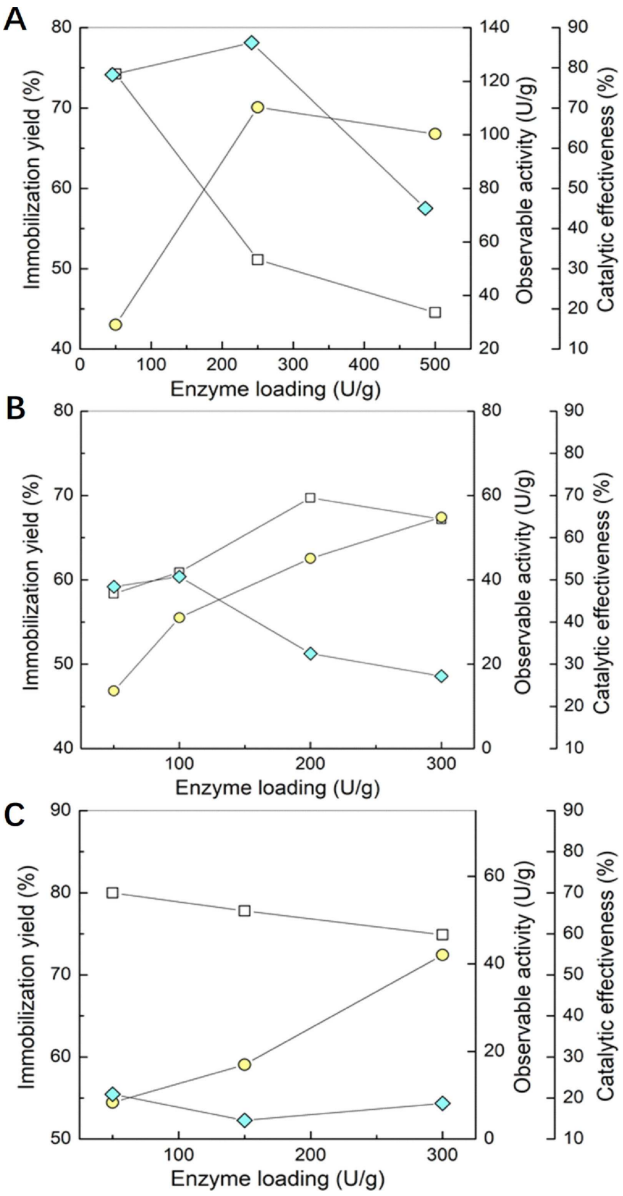

Figure 2. Immobilization of (A) Z–*Bl*ScP, (B) Z–*Cu*CbP and (C) Z–*Cc*CdP on ReliSorb SP400. Enzymes were immobilized directly from *E. coli* cell lysates. Carrier loading of 100 mg/mL was used for immobilization.

Single Z–enzyme immobilization

ReliSorb SP400 were used as carriers for immobilization. These are macro-porous polymethacrylate particles, roughly spherical in shape (75–200 μm diameter; 120 μm mean diameter) and with pore in 80–100 nm diameter.[26a] Sulfonate surface groups provide the negative charge that drives the binding of the Z_{basic2} module. Based on maximum protein size estimated from sequence and dimeric structure (i.e., Z–*Bl*ScP, ~11 nm; Z–*Cu*CbP, ~13 nm; Z–*Cc*CdP, ~14 nm), the pores of carriers were accessible to all the enzymes used. Taking into account that the Z–enzymes are, in general, bound to ReliSorb SP400 with excellent selectivity compared to proteins lacking the Z_{basic2} module,[24a,c] we omitted enzyme purification and immobilized Z–enzymes directly from *E. coli* cell lysate.

We summarize the results in Figure 2, showing the immobilization yield, activity, and catalytic effectiveness of the immobilized enzyme dependent on the enzyme loading. In anticipation of an enzyme co-immobilization in which the activity of Z–*Bl*ScP should be present in excess over the activities of Z–*Cu*CbP and *Cc*CdP (see later),[30] we examined a larger range of enzyme loadings for the Z–*Bl*ScP than for the other two enzymes. Although all the enzymes were adsorbed to the carrier in useful amount (≥50 U/g carrier), details of their immobilization behavior were yet enzyme-specific. This result indicated that factors other than the Z_{basic2} module influenced the enzyme tethering to the solid surface. Note: neither was this unexpected nor did it detract from the utility of Z_{basic2}-directed immobilization. Except for Z–*Cc*CdP as discussed later, the catalytic effectiveness of the immobilized enzymes was high (Z–*Bl*ScP: 85%) or usable (Z–*Cu*CbP: 52%) within a certain

loading range (Figure 2A,B). This was consistent with expectation for a largely oriented mode of surface binding via the Z_{basic2} module (Figure 1B and Figure S1) that retains accessibility and function of the enzyme active site broadly similar to in solution. However, for Z–*Bl*ScP and even more so for Z–*Cu*CbP, the catalytic effectiveness of the immobilized enzymes decreased dependent on the enzyme loading (Figure 2A,B). As all the activity assays employed substrates in large excess at fully saturating concentrations, the effect was unlikely to arise from limitations in substrate available to the immobilized enzyme in consequence of physical processes such as pore diffusion and partitioning.[33] A plausible reason for the observed loss of activity at high enzyme loading is that enzyme clustering occurs at suitable nucleation sites on the solid surface.[34] Such clustering could lead to an activity loss that is intrinsic (e.g., enzyme aggregation)[35] or is indirectly caused (e.g., by pore clogging).[36]

The rather low effectiveness of Z–*Cc*CdP (10–15%; Figure 2C) prompted us to further inquiry. The enzyme structure model revealed clusters of positive charge on the protein surface (Figure 3A) that could serve as sites/regions, alternative to Z_{basic2}, for the interaction with the solid surface. To dissect different surface-binding modes of Z–*Cc*CdP, we used the N-terminally His-tagged *Cc*CdP as reference and analyzed its adsorption to the ReliSorb SP400 carrier under variably stringent conditions of ionic strength (NaCl) and detergent (Tween 20) (Figure 3B and Figure S5). Enzyme immobilization just from 50 mM MES buffer was nearly quantitative (yield $\geq$95%). The yield was decreased to 44% and 27% in the presence of, respectively, 250 mM and 500 mM NaCl. Tween 20, whose addition was expected to interfere primarily with hydrophobic enzyme-surface interactions,[24b,37] showed a minor effect on the immobilization yield (Figure 3B). Comparing the Z–*Cc*CdP to His-tagged *Cc*CdP based on the immobilization yield at 250 mM NaCl revealed, that the overall binding of the Z–enzyme was dominated by the contribution from the Z_{basic2} module. Using 250 mM NaCl, indeed, the catalytic effectiveness of immobilized Z–*Cc*CdP was improved by 5-fold (~60%) compared to when no NaCl was added for immobilization (Figure 2C). Of note, such effect was achieved without compromising the immobilization yield (Figure 3B). These results indicate that, with a relatively small, rationally guided alteration in the immobilization conditions, the immobilization of Z–*Cc*CdP could be switched from a random process involving multiple modes of enzyme-surface interaction to an orientation-controlled process involving enzyme tethering primarily via the Z_{basic2} module.[24a,38] Moreover, oriented tethering is likely to reduce enzyme clustering and aggregation on the solid surface.[34,39] Thus, a spatially homogenous immobilization is enabled and this can also benefit the retention of full functionality in the immobilized enzymes.

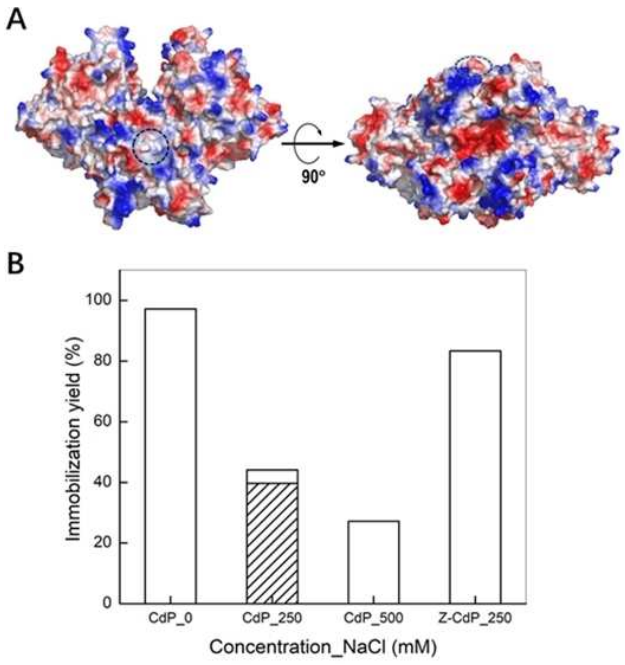

Figure 3. Oriented compared to random immobilization of Z–*Cc*CdP. (A) Surface charge distribution in a *Cc*CdP structure model (side and bottom view). The structure model was obtained from SWISS-MODEL using the experimental structure of *C. thermocellum* CdP (PDB entry 5NZ7) as the template (see Supporting Information). Note: *Cc*CdP (GenBank identifier CDZ24361.1) is 54% identical, and 75% similar, in sequence to the *C. thermocellum* CdP. Negative and positive charges are indicated in red and blue (PyMOL scale of $-/+64$). Charge neutral residues are shown in grey. The circled area shows the N-terminus where the Z_{basic2} module is attached. (B) Immobilization results. The His–*Cc*CdP and Z–*Cc*CdP (enzyme loading 100 U/g carrier) were immobilized in the absence or presence of NaCl (0.25–0.5 M). The hatched bar indicates the immobilization with additional 0.5% Tween 20.

Two-enzyme co-immobilization for cellobiose production

Coupled ScP and CbP can be used to synthesize cellobiose.[40] The two phosphorylases represent the first part of the envisioned enzyme cascade for the production of cello–oligosaccharides (Figure 1C). We co-immobilized the Z–*Bl*ScP and Z–*Cu*CbP on ReliSorb SP400, offering 140 U/g and 100 U/g, respectively. Enzyme loadings were chosen from Figure 2A,B for a useful compromise between the yield, activity and effectiveness. We considered furthermore that, according to the literature[9d,40b] and our own evidence on the performance of the enzyme cascade in solution (data not shown), the ScP activity should be present in about 2–3-fold excess over the CbP activity in order to achieve optimum in overall synthetic activity. Enzyme co-immobilization for a desired ratio of activities is challenging. Here, Z–*Bl*ScP was co-immobilized with Z–*Cu*CbP, offering both enzymes at the same time. An immobilization yield of 72% and 54% was obtained for Z–*Bl*ScP and Z–*Cu*CbP, respectively. Efficient co-immobilization of the enzymes was clearly demonstrated by SDS-PAGE (Figure 4A). The activity of immobilized Z–*Bl*ScP and Z–*Cu*CbP measured on carrier was 89 U/g and 33 U/g, respectively. A corresponding effectiveness of 88% and 61% was calculated. The enzyme activity ratio of 2.7 was thus finely tuned to the requirements for synthesis. Enzyme co-immobilization showed similar efficiency as the immobilization of the individual enzymes. There

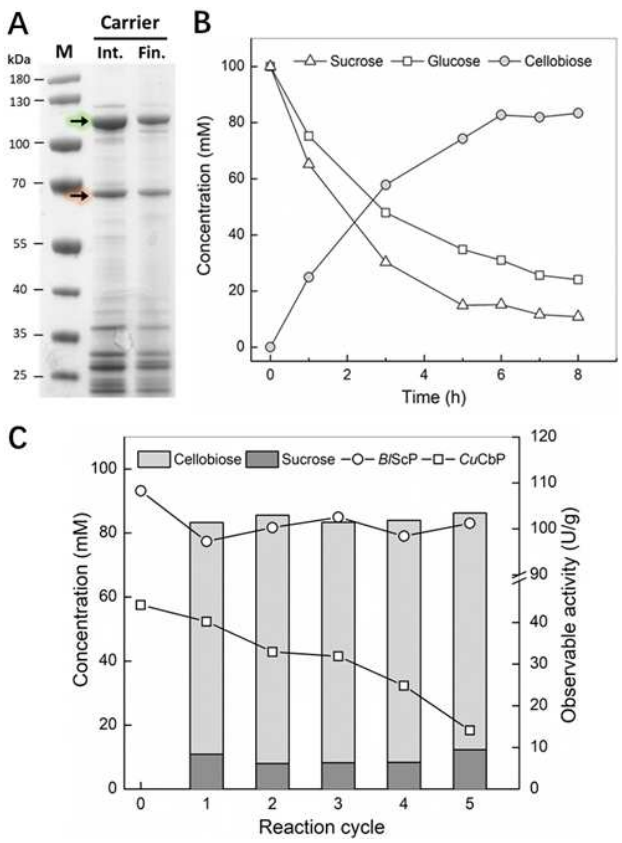

Figure 4. Synthesis of cellobiose by co-immobilized Z–*Bl*ScP and Z–*Cu*CbP. (A) SDS-PAGE of the immobilized Z–*Bl*ScP (pink) and Z–*Cu*CBP (green) on the carriers before and after reaction. Int., catalyst initially prepared with the two-enzyme co-immobilized; Fin., catalyst after 5 reaction cycles. (B) Time course on substrate conversion and cellobiose production in reaction using the co-immobilized catalyst (100 mM sucrose and glucose, 20 mM phosphate, activity of immobilized Z–*Bl*ScP and Z–*Cu*CbP in solution was 8 and 3 U/mL, 45 °C, pH 7.0). (C) Synthesis of cellobiose in repeated batch cycles integrated with the enzyme re-use: composition of mixture and enzyme activity on carriers at each cycle end. Conditions: 100 mM sucrose and glucose, 20 mM phosphate, 45 °C, pH 7.0. Starting activity of immobilized Z–*Bl*ScP and Z–*Cu*CbP in solution as 8 and 3 U/mL; 8 hrs for each cycle.

appeared to be no interference between the individual enzymes in becoming attached jointly to the solid carrier.

We applied the co-immobilized Z–*Bl*ScP (8 U/mL suspension) and Z–*Cu*CbP (3 U/mL suspension) to a batch synthesis of cellobiose, using 100 mM of each sucrose and glucose, and 20 mM phosphate. The reaction time course is as shown in Figure 4B. Cellobiose was released to ~80 mM within 6 hrs after which the reaction appeared to have reached apparent equilibrium. The initial production rate (~2.5 hrs) was around 25 mM/h. The overall productivity for conversion to apparent equilibrium was around 13 mM/h. Difference between the sucrose and glucose consumed (Figure 4B) was explained by the αGlc 1-*P* present in the mixture.

We tested afterwards the recycling of solid catalyst in repeated batch conversions under the conditions of Figure 4B. Five cycles were performed, each lasting 8 hrs. The final composition of the reaction mixture at the end of each cycle did not change as the cycle number increased (Figure 4C). We thus calculated a turnover number (*TN*) of ~1.9×10^5 (mol/mol) for the limiting Z–*Cu*CbP used. Using the soluble enzymes at equivalent volumetric activity, a *TN* of 7.4×10^4 (mol/mol) was obtained. A cycle number larger than 5 could be used to further enhance the *TN*, but at this stage, we think, the benefit of enzymes co-immobilization was made evident.

To explore the operational limits of the two-enzyme cascade on solid support, we performed direct assays on the residual activity of the immobilized enzymes after each cycle to analyze their operational stability. We show in Figure 4C that Z–*Bl*ScP was fully stable whereas Z–*Cu*CbP gradually decreased in activity. The activity loss was accompanied by the elution of Z–*Cu*CbP from the carrier, as shown in Figure 4A. CbP activity was detected in solution (data not shown). This result identified Z–enzyme elution as the actual cause of activity decrease in immobilized Z–*Cu*CbP. The relatively weak binding of Z–*Cu*CbP to ReliSorb SP400 might be explained by the orientation of the two Z_{basic2} modules relative to each other on the two parallel sides of the dimer structure (Figure S1A) which appears rather unfavorable for bivalent interaction with the solid surface. Moreover, the charge microenvironment of the Z_{basic2} module in the Z–*Cu*CbP structure might detract from its efficient (stable) immobilization. The *Cu*CbP surface features patches of negative charge in immediate vicinity (12–23 Å distance) to where a Z_{basic2} module would likely reside in the Z–enzyme fusion (Figure S2A). Besides the electrostatic repulsion generated from negatively charged surface of the carrier, the negatively charged protein areas could additionally destabilize the adsorbed state of Z–*Cu*CbP via competing intermolecular charge-charge interactions with the Z_{basic2} binding module. Increasing the number of Z_{basic2} modules on Z–*Cu*CbP through the construction of Z–Z–enzyme or Z–enzyme–Z fusions would represent a possible strategy to improve the operational stability of the immobilized enzyme.[26b] Besides this, various "individual" strategies of immobilization[14d,41] for Z–*Cu*CbP could be pursued to achieve co-immobilization with Z–*Bl*ScP.

Three-enzyme co-immobilization for cello–oligosaccharide production

To achieve good catalytic effectiveness for immobilized Z–*Cc*CdP (Figure 3B), we performed the three-enzyme co-immobilization in the presence of 250 mM NaCl. We loaded the Z–*Bl*ScP, Z–*Cu*CbP, and Z–*Cc*CdP at 300 U/g carrier, 100 U/g carrier and 150 U/g carrier, respectively. Besides the considerations of overall immobilization efficiency of each individual enzyme (Figure 2), we took into account that the DP-controlled synthesis of cello–oligosaccharides necessitates the three phosphorylases to be present in a balanced ratio of activities. In previous studies of the cascade reaction in solution,[30] we identified a favorable ratio 10:2:3 for the activities of ScP, CbP and CdP. The activity of the immobilized enzymes was 234 U/g (Z–*Bl*ScP), 49 U/g (Z–*Cu*CbP) and 74 U/g (Z–*Cc*CdP), thus well in line with the required ratio of activities for efficient production. It is worth emphasizing here that a similarly effective procedure of co-immobilization, based on the enzyme-specific strategies

of tethering to the solid support, would be quite challenging to establish.[6a,17a] Studies of the co-immobilization of just two glycoside phosphorylases or glycosyltransferases strongly support this contention.[42] In particular, balancing three phosphorylase activities in the final co-immobilized catalyst would require optimization of a set of highly interconnected immobilization parameters. Through SDS-PAGE (Figure 5A), we show the selective co-immobilization of the three phosphorylases directly from their corresponding protein bands in the gel. The high purity of the three-enzyme system eluted from carrier is noted. Catalytic effectiveness of immobilized enzyme exceeded 50% for all the three phosphorylases. An efficient approach to "multi-enzyme system co-immobilization" is thus demonstrated in this study.

We then applied the three-phosphorylase co-immobilized catalyst for the synthesis of short-chain (soluble) cello–oligosaccharides. The actual product is a mixture of the cello–oligosaccharides of different DPs. We targeted the cello–oligosaccharides of DP 3–6. Upper limit of DP 6 is to prevent soluble product loss into insoluble cellulose material. We used the conditions previously established for the enzymatic cascade reaction in solution: 200 mM sucrose, 65 mM glucose and 50 mM phosphate.[30] The volumetric activity of the immobilized enzymes in suspension was 9 U/mL for Z–*Bl*ScP, 2 U/mL for Z–*Cu*CbP and 3 U/mL for Z–*Cc*CdP. As shown in Figure 5B, ~90% of the initial sucrose was converted within 3 hrs and cello–oligosaccharides were released concomitantly. The soluble product accumulated at a total concentration of 25 g/L. The oligosaccharide distribution in the product was, per weight, 32% DP3, 32% DP4, 24% DP5 and 12% DP6. Here, we noted that the molar yield of soluble cello–oligosaccharides was considerably less (56 mol.%) than expected from the sucrose conversion. As shown in Figure S6A, the effect is explained by the insoluble product formation. Using co-immobilized enzymes, product precipitation occurred at a higher rate than the study of cello–oligosaccharide synthesis with the soluble enzymes had suggested.[30] Difference in behavior of soluble and immobilized enzyme cascades is not straightforward to explain and certainly warrants further mechanistic inquiry. The comparably high volumetric reaction rates in the confinement of the porous particle might be a relevant factor. However, here we prioritized avoiding the insoluble product, because its separation from the solid catalyst is challenging (Figure S6B). We used evidence on the time dependence of product precipitation (Figure S6A) to limit the reaction time to maximum 1.5 hrs. Under these conditions, the expected total cello–oligosaccharide concentration is only about half of that obtained at 3 hrs (Figure 5B), but no insoluble product will be formed.

Recyclability of the co-immobilized catalyst was examined in five consecutive batch reactions, each cycle lasting 1.5 hrs. The total amount of cello–oligosaccharides released was as expected (~12 g/L; ~30% molar yield) and the DP distribution in the product was largely constant in each cycle, as shown in Figure 6. We applied SDS-PAGE to compare the composition of the co-immobilized enzymes before and after these five reactions. As already noted from the co-immobilized Z–*Bl*ScP and Z–*Cu*CbP (Figure 4A), there was also a substantial release of Z–*Cu*CbP from the carrier over the 5 cycles of reaction. Z–*Bl*ScP and Z–*Cc*CdP were bound more strongly by comparison (Figure 5A). Visualization of the surface charge distribution in enzyme structure models (Figure 3 and Figure S2) supports the idea that *Cu*CbP may be too strongly negatively charged to become effectively attached to a negatively charged surface via a single Z_{basic2} module. Tentatively, *Bl*ScP and *Cc*CdP may be more suitable on the criterion for this surface charge.

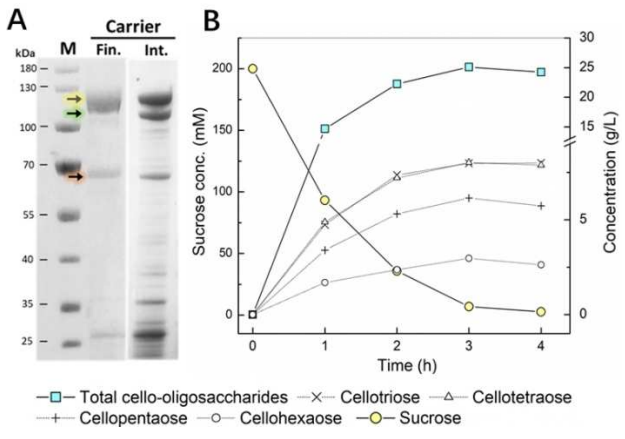

Figure 5. Synthesis of cello–oligosaccharides by co-immobilized Z–*Bl*ScP, Z–*Cu*CbP and Z–*Cc*CdP. (A) SDS-PAGE of the immobilized Z–*Bl*ScP (pink), Z–*Cu*CbP (green), Z–*Cc*CdP (yellow) on the carriers before and after reaction. Int., catalyst initially prepared with three-enzyme co-immobilized; Fin., catalyst after five reaction cycles. (B) Time course of sucrose conversion and soluble cello–oligosaccharides release in enzymatic reaction using co-immobilized catalyst (200 mM sucrose, 65 mM glucose, 50 mM phosphate, Z–*Bl*ScP, Z–*Cu*CbP, Z–*Cc*CdP of 9, 2 and 3 U/mL in suspension, 45 °C, pH 7.0).

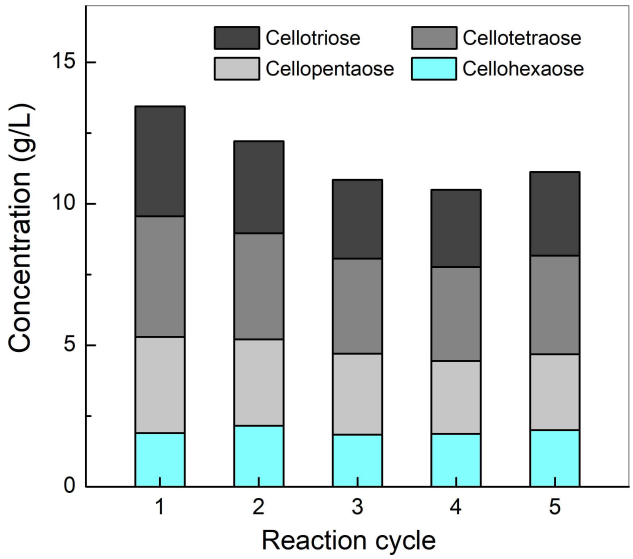

Figure 6. Synthesis of soluble cello–oligosaccharides in repeated batch cycles integrated with enzyme re-use. Conditions: 200 mM sucrose, 65 mM glucose, 50 mM phosphate, 45 °C, pH 7.0; Z–*Bl*ScP (9 U/mL), Z–*Cu*CbP (2 U/mL), and Z–*Cc*CdP (3 U/mL) co-immobilized on ReliSorb SP 400 was used; 1.5 hrs for each cycle.

Conclusions

We demonstrate a cascade of three glucoside phosphorylases co-immobilized on solid support for the biocatalytic production of cello–oligosaccharides (DP $\leq$ 6) with integrated re-use of enzymes. The challenge to co-immobilize multiple enzymes at a defined ratio of their individual activities, which is absolutely critical for the DP-controlled synthesis of the cello–oligosaccharides,[23,24] was effectively overcome by using a modular fusion protein approach. Exploiting a uniform principle of surface tethering via the binding module Z_{basic2}, a convenient and well programmable co-immobilization of Z–*Bl*ScP, Z–*Cu*CbP and Z–*Cc*CdP directly from their corresponding *E. coli* cell lysates was made possible. Limitation on the operational stability of the immobilized Z–*Cu*CbP arose due to enzyme elution from the solid carrier. Fusing a second Z_{basic2} module to Z–*Cu*CbP can improve the binding, as suggested from an earlier study of Z_{basic2} variants of the ScP from *Leuconostoc mesenteroides*.[26b] The issue encountered with Z–*Cu*CbP does not, therefore, detract from the conceptual appeal and the potential general utility of the approach. The principle of Z_{basic2}-directed multienzyme co-immobilization on anionic supports appears to be broadly applicable to biocatalytic cascade reactions.[6a,16b,43] More specifically in the oligosaccharide and specialty carbohydrate synthesis, its use might be extended to various cascades of glycoside phosphorylases[9d,44] or glycosyltransferases[9h,45] that have shown promising performances when used as soluble enzymes.

Experimental Section

Chemicals and materials

ReliSorb SP400 was from Resindion S.R.L. (Binasco, Italy). According to the technical data sheet from the manufacturer, the carrier's moisture content is 72% (w/w). Wet carrier weight is used throughout. Unless stated, the chemicals and oligonucleotide primers were from Sigma-Aldrich (Vienna, Austria) or Carl Roth (Karlsruhe, Germany). Reagent-grade cello–oligosaccharides of DP 2–6 were from Carbosynth (Compton, Berkshire, U.K.).

Enzymes

Chimeric forms of *Bl*ScP, *Cu*CbP and *Cc*CdP were constructed that harbor the binding module Z_{basic2} at the native enzyme's N-terminus. The cloning work, protein expression and purification are described in full details in the Supporting Information. Enzyme structure models were constructed using SWISS-MODEL with default parameters. The molecular surface charge distributions in enzyme structure models were visualized with PyMOL.

Enzyme immobilization

Reported procedure for immobilizing Z-enzymes directly from *E. coli* cell extract was used.[24c] A MES buffer (50 mM), pH 7.0, was used. Note: the Z-enzyme accounted for roughly 12–17% of total protein present in the cell extract. Here, *E. coli* cell extract was optionally supplemented with 0.25 M NaCl or with additional 0.5% (v/v) Tween 20, as indicated under Results. For immobilization, which was done in 1 mL volume, 100 mg carriers (dry material) were mixed with suitably diluted cell extract to load an enzyme activity of 50–500 U/g carrier. The suspensions were incubated in an end-over-end rotator (20 rpm) at 25 °C for 1 hr. After that, samples were taken from the supernatant after sedimentation of the beads. Enzyme activity (in U/mL) in the supernatant was determined. The enzyme bound to the carrier was checked by SDS-PAGE.

Enzyme co-immobilization was performed similarly as described above for single enzyme immobilization. Before immobilization, the individual cell extracts of Z–*Bl*ScP and Z–*Cu*CbP were mixed to achieve a loading activity of 140 U/g and 100 U/g, respectively. Similarly, the cell extracts of Z–*Bl*ScP (300 U/g), Z–*Cu*CbP (100 U/g), and Z–*Cc*CdP (150 U/g) were mixed to give the appropriate loading of activities. Additional 0.25 M NaCl was added. For co-immobilization, which was done in 6 mL total volume, 200 mg of carriers were used. Incubations were done in an end-over-end rotator (20 rpm) at 25 °C for 2 hrs. The co-immobilized carriers were separated by centrifugation (10,000 rpm), and washed with 5 mL of loading buffer, and stored at 4 °C until use.

The immobilization yield (%) was calculated as $100\times(a_0-a)/a_0$, where a_0 is the initial enzyme activity and a is the enzyme activity in supernatant after immobilization. The catalytic effectiveness (η) was calculated as the ratio of the observable enzyme activity on the carrier (U/g) and the theoretically immobilized enzyme activity which was calculated from the difference (a_0-a).

Activity assay

Assays of soluble enzymes. The activity of ScP was determined in the direction of sucrose phosphorolysis (50 mM sucrose; 50 mM phosphate; pH 7.0, 45 °C). The αGlc1-*P* released was monitored continuously by a coupled enzyme assay.[46] One unit (U) of activity is the enzyme amount producing 1 μmol αGlc1-*P*/min under the conditions employed. The activity of Z–CbP or CdP was determined in the direction of cellobiose or cellodextrin synthesis (50 mM αGlc1-*P*; 50 mM glucose or cellobiose; pH 7.0, 45 °C), respectively, using method from literature.[29] One unit (U) of activity is the enzyme amount producing 1 μmol phosphate/min under the conditions employed.

Assays of the individually immobilized enzymes. The activity assays described above were used for immobilized CbP and CdP. Carriers (10 mg) were incubated in 1 mL substrate solution under an agitation rate of 900 rpm using a ThermoMixer C (Eppendorf, Vienna, Austria). The phosphate released in samples from the incubation was measured. The activity of Z–*Bl*ScP immobilized on solid carrier was measured with modifications of the assay for the soluble enzyme. Samples (20 μL) were periodically collected over a period of 10 min from the incubation of the solid carriers. The αGlc1-*P* released was measured discontinuously by the coupled enzyme assay.[47]

Assays of the co-immobilized enzymes. The activities of Z–*Bl*ScP and Z–*Cu*CbP co-immobilized on solid carrier were measured as described above for the individually immobilized enzymes. Determination of the immobilized Z–*Cc*CdP activity required an assay different from the ones described above, so that possible interference from the simultaneously present Z–*Cu*CbP activity was eliminated. Therefore, the immobilized Z–*Cc*CdP activity was measured in the direction of oligosaccharide synthesis (50 mM αGlc1-*P*, pH 7.0, 45 °C) using *p*-nitrophenyl β-D-cellobioside (50 mM) as the acceptor substrate. The *p*-nitrophenyl β-D-cellobioside is not a substrate for the phosphorolysis reaction by Z–*Cu*CbP. In the calculation of the immobilized enzyme activity, we considered that for soluble Z–*Cc*CdP the activity with *p*-nitrophenyl β-D-

cellobioside is 1.2-fold that with cellobiose. It was assumed that the same factor in activity applies to the immobilized enzyme.

Cellobiose and cello–oligosaccharide synthesis

All reactions were carried out at 45 °C using an agitation rate of 900 rpm (ThermoMixer C). A total volume of 1.0 mL was used.

For cellobiose synthesis, the reaction contained 100 mM sucrose and glucose, 20 mM phosphate in MES buffer (50 mM, pH 7.0). For cello–oligosaccharide synthesis, the reaction contained 200 mM sucrose, 65 mM glucose, and 50 mM phosphate in MES buffer (50 mM, pH 7.0). Both reactions were started by adding the enzymes co-immobilized on solid support. The added activity of Z–*Bl*ScP and Z–*Cu*CbP was 8 U/mL and 3 U/mL, respectively. The added activity of Z–*Bl*ScP, Z–*Cu*CbP and Z–*Cc*CdP was 9 U/mL, 2 U/mL and 3 U/mL, respectively. Samples (50 μL) were taken from the reaction periodically while the beads were still in suspension.

To test the recyclability of the immobilized enzymes, solid carriers were recovered by centrifugation (10,000 rpm, 5 min) after each cycle. The carriers were washed with loading buffer and added to fresh substrate solution to start a new reaction. The cycle was repeated several times.

Analytics

Samples from the reaction were centrifuged (15,000 rpm, 10 min). The supernatant was heated (95 °C, 5 min) and centrifuged again before analysis. Cellobiose and cello–oligosaccharides (DP 3–6) were analyzed by HPLC on a Hitachi LaChrom HPLC system (Merck, Darmstadt, Germany) using a Luna 5 μm NH_2 column (100 Å, 250× 4.6 mm, Phenomenex, Aschaffenburg, Germany) operated at 40 °C. Acetonitrile–water (67.5:32.5, by volume) was used as eluent at a flow rate of 1.5 mL/min. Glucose and fructose were analyzed using the same HPLC set-up but with an Aminex HPX-87C Column (300× 7.8 mm, Bio-Rad Laboratories, Vienna, Austria) operated at 80 °C. Milli-Q water was used as eluent at a flow rate of 0.4 mL/min. Alternatively, reaction mixtures from cellobiose synthesis were analyzed with a YMC-Pack Polyamine II/S-5 μm/12 nm column (250×4.6 mm, YMC America, Allentown, US) with a guard column (20×4.0 mm) installed. Acetonitrile–water (75:25, by volume) was used as eluent at a flow rate of 1.0 mL/min. Refractive index detection was used to quantitate the compounds. Calibration was done with the authentic standards. Phosphate was measured with a colorimetric assay.[29]

In cello–oligosaccharide synthesis, the molar yield was defined as the mole ratio of glucosyl units in the cello–oligosaccharides formed to the sucrose added to the reaction. The soluble mole ratio is the ratio of glucosyl units in soluble cello–oligosaccharides (including cellobiose) to the glucosyl units transferred from αGlc1-*P* in the overall reaction. A soluble mole ratio of 1 indicates 100% soluble products.

Data accessibility statement

Data obtained in the current study are available from the DOI 10.5281/zenodo.3564235.

Acknowledgements

This project has received funding from the European Union's Horizon 2020 research and innovation programme under grant agreement No 761030 (CARBAFIN). B.D. acknowledges support from Erasmus + for student exchange from University of Zagreb to Graz University of Technology. J.M.B. acknowledges the Government of Community of Madrid (2018-T1/BIO-10200). The thematic framework of Graz University of Technology Lead Project "PorousMaterials@Work" is acknowledged.

Keywords: biocatalytic cascade · biotransformation · enzyme immobilization · cello–oligosaccharides · phosphorylases

[1] a) F. Lopez-Gallego, C. Schmidt-Dannert, *Curr. Opin. Chem. Biol.* **2010**, *14*, 174–183; b) J. Muschiol, C. Peters, N. Oberleitner, M. D. Mihovilovic, U. T. Bornscheuer, F. Rudroff, *Chem. Commun.* **2015**, *51*, 5798–5811.
[2] a) S. P. France, L. J. Hepworth, N. J. Turner, S. L. Flitsch, *ACS Catal.* **2017**, *7*, 710–724; b) P. A. Santacoloma, G. Sin, K. V. Gernaey, J. M. Woodley, *Org. Process Res. Dev.* **2011**, *15*, 203–212.
[3] a) R. Metzner, W. Hummel, F. Wetterich, B. König, H. Gröger, *Org. Process Res. Dev.* **2015**, *19*, 635–638; b) Y. Wang, H. Zhao, *Catalysts* **2016**, *6*, 194; c) J. M. Sperl, V. Sieber, *ACS Catal.* **2018**, *8*, 2385–2396.
[4] J. H. Schrittwieser, S. Velikogne, M. Hall, W. Kroutil, *Chem. Rev.* **2018**, *118*, 270–348.
[5] a) P. Gruber, M. P. C. Marques, B. O'Sullivan, F. Baganz, R. Wohlgemuth, N. Szita, *Biotechnol. J.* **2017**, *12*, 1700030; b) P. Qi, C. You, Y. H. P. Zhang, *ACS Catal.* **2014**, *4*, 1311–1317.
[6] a) E. T. Hwang, S. Lee, *ACS Catal.* **2019**, *9*, 4402–4425; b) R. Abu, J. M. Woodley, *ChemCatChem* **2015**, *7*, 3094–3105; c) E. Ricca, B. Brucher, J. H. Schrittwieser, *Adv. Synth. Catal.* **2011**, *353*, 2239–2262.
[7] A. V. Ruales-Salcedo, J. C. Higuita, J. Fontalvo, J. M. Woodley, *J. Biosci.* **2019**, *74*, 77–84.
[8] a) I. Oroz-Guinea, E. García-Junceda, *Curr. Opin. Chem. Biol.* **2013**, *17*, 236–249; b) S. Wu, Z. Li, *ChemCatChem* **2018**, *10*, 2164–2178.
[9] a) H. Yu, X. Chen, *Org. Biomol. Chem.* **2016**, *14*, 2809–2818; b) G. Pergolizzi, S. Kuhaudomlarp, E. Kalita, R. A. Field, *Protein Pept. Lett.* **2017**, *24*, 696–709; c) W. Li, J. B. McArthur, X. Chen, *Carbohydr. Res.* **2019**, *472*, 86–97; d) C. Luley-Goedl, B. Nidetzky, *Biotechnol. J.* **2010**, *5*, 1324–1338; e) W.-D. Fessner, *New Biotechnol.* **2015**, *32*, 658–664; f) J. Nahalka, Z. Liu, X. Chen, P. G. Wang, *Chem. Eur. J.* **2003**, *9*, 372–377; g) R. R. Rosencrantz, B. Lange, L. Elling in *Cascade Biocatalysis: Integrating Stereoselective and Environmentally Friendly Reactions* (Eds.: S. Riva, W.-D. Fessner), Wiley-VCH, **2014**, pp. 133–160; h) B. Nidetzky, A. Gutmann, C. Zhong, *ACS Catal.* **2018**, *8*, 6283–6300.
[10] a) Y. Chen, Y. Li, H. Yu, G. Sugiarto, V. Thon, J. Hwang, L. Ding, L. Hie, X. Chen, *Angew. Chem. Int. Ed.* **2013**, *52*, 11852–11856; *Angew. Chem.* **2013**, *125*, 12068–12072; b) U. Bhaskar, G. Li, L. Fu, A. Onishi, M. Suflita, J. S. Dordick, R. J. Linhardt, *Carbohydr. Polym.* **2015**, *122*, 399–407; c) X. Zhang, R. J. Linhardt in *Chemical Biology of Glycoproteins* (Eds.: Z.-P. Tan, L.-X. Wang), Royal Society of Chemistry, **2017**, pp. 233–252; d) J. Liu, R. J. Linhardt, *Nat. Prod. Rep.* **2014**, *31*, 1676–1685.
[11] a) H. Yu, H. A. Chokhawala, S. Huang, X. Chen, *Nat. Protoc.* **2006**, *1*, 2485–2492; b) X. Chen in *Advances in Carbohydrate Chemistry and Biochemistry, Vol. 72* (Eds.: D. C. Baker, D. Horton), Academic Press, **2015**, pp. 113–190; c) H. Yu, K. Lau, Y. Li, G. Sugiarto, X. Chen, *Curr Protoc. Chem. Biol.* **2012**, *4*, 233–247; d) B. Zeuner, D. Teze, J. Muschiol, A. S. Meyer, *Molecules* **2019**, *24*, 2033; e) B. Petschacher, B. Nidetzky, *J. Biotechnol.* **2016**, *235*, 61–83; f) H. Yu, Y. Li, Z. Wu, L. Li, J. Zeng, C. Zhao, Y. Wu, N. Tasnima, J. Wang, H. Liu, M. R. Gadi, W. Guan, P. G. Wang, X. Chen, *Chem. Commun.* **2017**, *53*, 11012–11015.
[12] a) R. Heinzler, T. Fischöder, L. Elling, M. Franzreb, *Adv. Synth. Catal.* **2019**, *361*, 4506–4516; b) T. Fischoder, S. Cajic, U. Reichl, E. Rapp, L. Elling, *Biotechnol. J.* **2019**, *14*, e1800305; c) J. Zhang, C. Chen, M. R. Gadi, C. Gibbons, Y. Guo, X. Cao, G. Edmunds, S. Wang, D. Liu, J. Yu, L. Wen, P. G. Wang, *Angew. Chem. Int. Ed.* **2018**, *57*, 16638–16642; *Angew. Chem.* **2018**, *130*, 16880–16884.
[13] J.-M. Choi, S.-S. Han, H.-S. Kim, *Biotechnol. Adv.* **2015**, *33*, 1443–1454.

[14] a) R. A. Sheldon, S. van Pelt, *Chem. Soc. Rev.* **2013**, *42*, 6223–6235; b) R. DiCosimo, J. McAuliffe, A. J. Poulose, G. Bohlmann, *Chem. Soc. Rev.* **2013**, *42*, 6437–6474; c) J. M. Bolivar, I. Eisl, B. Nidetzky, *Catal. Today* **2016**, *259*, 66–80; d) C. Garcia-Galan, Á. Berenguer-Murcia, R. Fernández-Lafuente, R. C. Rodrigues, *Adv. Synth. Catal.* **2011**, *353*, 2885–2904.
[15] a) R. C. Rodrigues, C. Ortiz, Á. Berenguer-Murcia, R. Torres, R. Fernández-Lafuente, *Chem. Soc. Rev.* **2013**, *42*, 6290–6307; b) S. Ren, C. Li, X. Jiao, S. Jia, Y. Jiang, M. Bilal, J. Cui, *Chem. Eng. J.* **2019**, *373*, 1254–1278.
[16] a) Y. Zhu, Q. Chen, L. Shao, Y. Jia, X. Zhang, *React. Chem. Eng.* **2019**, 10.1039/c9re00217k; b) Q. Ji, B. Wang, J. Tan, L. Zhu, L. Li, *Process Biochem.* **2016**, *51*, 1193–1203.
[17] a) F. Kazenwadel, M. Franzreb, B. E. Rapp, *Anal. Methods* **2015**, *7*, 4030–4037; b) L. Betancor, H. Luckarift, *Biotechnol. Genet. Eng. Rev.* **2010**, *27*, 95–114.
[18] a) S. Velasco-Lozano, F. López-Gallego, *Biocatal. Biotransform.* **2018**, *36*, 184–194; b) N. S. Rios, S. Arana-Peña, C. Mendez-Sanchez, C. Ortiz, L. R. B. Gonçalves, R. Fernández-Lafuente, *Catalysts* **2019**, *9*, 487; c) S. Schoffelen, J. C. M. van Hest, *Curr. Opin. Struct. Biol.* **2013**, *23*, 613–621.
[19] S. Velasco-Lozano, A. I. Benítez-Mateos, F. López-Gallego, *Angew. Chem. Int. Ed.* **2017**, *56*, 771–775; *Angew. Chem.* **2017**, *129*, 789–793.
[20] a) C. Schmid-Dannert, F. López-Gallego, *Curr. Opin. Chem. Biol.* **2019**, *49*, 97–104; b) A. Giannakopoulou, E. Gkantzou, A. Polydera, H. Stamatis, *Trends Biotechnol.* **2019**, 10.1016/j.tibtech.2019.07.010.
[21] a) C. Mateo, J. M. Palomo, G. Fernandez-Lorente, J. M. Guisan, R. Fernández-Lafuente, *Enzyme Microb. Technol.* **2007**, *40*, 1451–1463; b) Y. Zhang, J. Ge, Z. Liu, *ACS Catal.* **2015**, *5*, 4503–4513.
[22] X. Chen, J. Fang, J. Zhang, Z. Liu, J. Shao, P. Kowal, P. Andreana, P. G. Wang, *J. Am. Chem. Soc.* **2001**, *123*, 2081–2082.
[23] a) F. Khan, M. He, M. J. Taussig, *Anal. Chem.* **2006**, *78*, 3072–3079; b) W. Liu, L. Wang, R. Jiang, *Top. Catal.* **2012**, *55*, 1146–1156; c) C. Ley, D. Holtmann, K.-M. Mangold, J. Schrader, *Colloids Surf. B* **2011**, *88*, 539–551.
[24] a) J. Wiesbauer, J. M. Bolivar, M. Mueller, M. Schiller, B. Nidetzky, *ChemCatChem* **2011**, *3*, 1299–1303; b) J. M. Bolivar, B. Nidetzky, *Langmuir* **2012**, *28*, 10040–10049; c) J. M. Bolivar, B. Nidetzky, *Biotechnol. Bioeng.* **2012**, *109*, 1490–1498; d) J. M. Bolivar, S. Schelch, T. Mayr, B. Nidetzky, *ACS Catal.* **2015**, *5*, 5984–5993.
[25] M. Hartmann, X. Kostrov, *Chem. Soc. Rev.* **2013**, *42*, 6277–6289.
[26] a) D. Valikhani, J. M. Bolivar, A. Dennig, B. Nidetzky, *Biotechnol. Bioeng.* **2018**, *115*, 2416–2425; b) D. Valikhani, J. M. Bolivar, M. Pfeiffer, B. Nidetzky, *ChemCatChem* **2017**, *9*, 161–166; c) J. M. Bolivar, C. Luley-Goedl, E. Leitner, T. Sawangwan, B. Nidetzky, *J. Biotechnol.* **2017**, *257*, 131–138.
[27] a) S. Patel, A. Goyal, *World J. Microbiol. Biotechnol.* **2011**, *27*, 1119–1128; b) S. I. Mussatto, I. M. Mancilha, *Carbohydr. Polym.* **2007**, *68*, 587–597; c) H. J. Flint, E. A. Bayer, M. T. Rincon, R. Lamed, B. A. White, *Nat. Rev. Microbiol.* **2008**, *6*, 121–131.
[28] a) M. Otsuka, A. Ishida, Y. Nakayama, M. Saito, M. Yamazaki, H. Murakami, Y. Nakamura, M. Matsumoto, K. Mamoto, R. Takada, *Anim. Sci. J.* **2004**, *75*, 225–229; b) Y. Uyeno, K. Kawashima, T. Hasunuma, W. Wakimoto, M. Noda, S. Nagashima, K. Akiyama, M. Tabata, S. Kushibiki, *Livest. Sci.* **2013**, *153*, 88–93.
[29] C. Zhong, C. Luley-Goedl, B. Nidetzky, *Biotechnol. Bioeng.* **2019**, *116*, 2146–2155.
[30] C. Zhong, B. Nidetzky, *Biotechnol. J.* **2019**, 1900349.
[31] Y. P. Zhang, L. R. Lynd, *Appl. Microbiol. Biotechnol.* **2006**, *70*, 123–129.
[32] D. M. Petrovic, I. Kok, A. J. Woortman, J. Ciric, K. Loos, *Anal. Chem.* **2015**, *87*, 9639–9646.
[33] M. M. Hossain, D. D. Do, J. E. Bailey, *AIChE J.* **1986**, *32*, 1088–1098.
[34] H. Zaak, E.-H. Siar, J. F. Kornecki, L. Fernandez-Lopez, S. G. Pedrero, J. J. Virgen-Ortíz, R. Fernandez-Lafuente, *Process Biochem.* **2017**, *56*, 117–123.
[35] R. Fernandez-Lafuente, *Enzyme Microb. Technol.* **2009**, *45*, 405–418.
[36] A. A. Homaei, R. Sariri, F. Vianello, R. Stevanato, *J. Chem. Biol.* **2013**, *6*, 185–205.
[37] D.-J. Seo, H. Fujita, A. Sakoda, *Adsorption* **2011**, *17*, 813–822.
[38] J. C. Y. Wu, C. H. Hutchings, M. J. Lindsay, C. J. Werner, B. C. Bundy, *J. Biotechnol.* **2015**, *193*, 83–90.
[39] a) S. Mittal, L. R. Singh, *PLoS One* **2013**, *8*, e78936; b) L. Fernandez-Lopez, S. G. Pedrero, N. Lopez-Carrobles, B. C. Gorines, J. J. Virgen-Ortíz, R. Fernandez-Lafuente, *Enzyme Microb. Technol.* **2017**, *98*, 18–25.
[40] a) C. Zhong, P. Wei, Y.-H. P. Zhang, *Chem. Eng. Sci.* **2017**, *161*, 159–166; b) M. Kitaoka, T. Sasaki, H. Taniguchi, *J. Jpn. Soc. Starch Sci.* **1992**, *39*, 281–283.
[41] a) F. Jia, B. Narasimhan, S. Mallapragada, *Biotechnol. Bioeng.* **2014**, *111*, 209–222; b) S. Arana-Peña, C. Mendez-Sanchez, N. S. Rios, C. Ortiz, L. R. B. Gonçalves, R. Fernández-Lafuente, *Int. J. Biol. Macromol.* **2019**, *131*, 989–997.
[42] a) Q. Dong, L.-M. Ouyang, H.-L. Yu, J.-H. Xu, *Carbohydr. Res.* **2010**, *345*, 1622–1626; b) C. You, H. Chen, S. Myung, N. Sathitsuksanoh, H. Ma, X.-Z. Zhang, J. Li, Y.-H. P. Zhang, *Proc. Natl. Acad. Sci. USA* **2013**, *110*, 7182–7187; c) L. Trobo-Maseda, A. H. Orrego, S. Moreno-Perez, G. Fernandez-Lorrente, J. M. Guisan, J. Rocha-Martin, *Appl. Microbiol. Biotechnol.* **2018**, *102*, 773–787; d) A. Abi, A. Wang, H. J. Jördening, *Appl. Biochem. Biotechnol.* **2018**, *186*, 861–876.
[43] C. Schmidt-Dannert, F. Lopez-Gallego, *Microb. Biotechnol.* **2016**, *9*, 601–609.
[44] a) H. Nakai, M. Kitaoka, B. Svensson, K. Ohtsubo, *Curr. Opin. Chem. Biol.* **2013**, *17*, 301–309; b) E. C. O'Neill, R. A. Field, *Carbohydr. Res.* **2015**, *403*, 23–37; c) K. Loos, J.-i. Kadokawa in *Enzymatic Polymerization towards Green Polymer Chemistry* (Eds.: S. Kobayashi, H. Uyama, J.-i. Kadokawa), Springer Singapore, **2019**, pp. 47–87.
[45] a) H. Yu, H. Chokhawala, R. Karpel, H. Yu, B. Wu, J. Zhang, Y. Zhang, Q. Jia, X. Chen, *J. Am. Chem. Soc.* **2005**, *127*, 17618–17619; b) A. Gutmann, A. Lepak, M. Diricks, T. Desmet, B. Nidetzky, *Biotechnol. J.* **2017**, *12*; c) K. Schmölzer, M. Lemmerer, B. Nidetzky, *Biotechnol. Bioeng.* **2018**, *115*, 545–556; d) A. Gutmann, L. Bungaruang, H. Weber, M. Leypold, R. Breinbauer, B. Nidetzky, *Green Chem.* **2014**, *16*, 4417–4425.
[46] C. Eis, B. Nidetzky, *Biochem. J.* **1999**, *341*, 385–393.
[47] P. Wildberger, G. A. Aish, D. L. Jakeman, L. Brecker, B. Nidetzky, *Biochem. Biophys. Rep.* **2015**, *2*, 36–44.

Manuscript received: October 17, 2019
Revised manuscript received: November 17, 2019
Accepted manuscript online: December 3, 2019
Version of record online: January 22, 2020